nature physics

LETTERS

PUBLISHED ONLINE: 13 MAY 2012 | DOI: 10.1038/NPHYS2318

Equal-spin Andreev reflection and long-range coherent transport in high-temperature superconductor/half-metallic ferromagnet junctions

C. Visani[1,2], Z. Sefrioui[3,4], J. Tornos[3,4], C. Leon[3,4], J. Briatico[1,2], M. Bibes[1,2], A. Barthélémy[1,2], J. Santamaría[3,4] and Javier E. Villegas[1,2]*

Conventional superconductivity is incompatible with ferromagnetism, because the magnetic exchange field tends to spin-polarize electrons and breaks apart the opposite-spin singlet Cooper pairs[1]. Yet, the possibility of a long-range penetration of superconducting correlations into strong ferromagnets has been evinced by experiments that found Josephson coupling between superconducting electrodes separated afar by a ferromagnetic spacer[2–7]. This is considered a proof of the emergence at the superconductor/ferromagnetic (S/F) interfaces of equal-spin triplet pairing, which is immune to the exchange field and can therefore propagate over long distances into the F (ref. 8). This effect bears much fundamental interest and potential for spintronic applications[9]. However, a spectroscopic signature of the underlying microscopic mechanisms has remained elusive. Here we do show this type of evidence, notably in a S/F system for which the possible appearance of equal-spin triplet pairing is controversial[10–12]: heterostructures that combine a half-metallic F ($La_{0.7}Ca_{0.3}MnO_3$) with a *d*-wave S ($YBa_2Cu_3O_7$). We found quasiparticle and electron interference effects in the conductance across the S/F interfaces that directly demonstrate the long-range propagation across $La_{0.7}Ca_{0.3}MnO_3$ of superconducting correlations, and imply the occurrence of unconventional equal-spin Andreev reflection. This allows for an understanding of the unusual proximity behaviour observed in this type of heterostructures[12,13].

The proximity effect, usually described as the penetration or 'leakage' of the superconducting condensate from a S into an overlaying normal metal (N), is on a microscopic level the result of two processes. The first one is the Andreev reflection[14], through which a normal electron incident into the S/N interface is paired with an electron inside the Fermi sea by the S energy gap, leaving a hole excitation that propagates backwards from the interface. In the conventional picture, the incident electron and the reflected hole must have opposite spins. The second process is the coherent propagation into the N material of the resulting hole/electron phase-conjugated pair[15]. The latter carries the superconducting correlations into the N, leading to a finite condensation amplitude over a certain length scale ξ_N, as schematically shown in Fig. 1a. In the N, such coherent propagation is limited only by the usual dephasing mechanisms and diverges at zero temperature (T): for diffusive systems $\xi_N = \sqrt{\hbar D/2\pi KT}$ and for ballistic ones $\xi_N = \hbar v_F/2\pi KT$, where D is the electronic diffusion constant, K is the Boltzmann constant and v_F is the Fermi velocity[15]. In clean metals, at low temperatures, ξ_N can be micrometres long. If the material in contact with the S is a F, the two processes above—and therefore the conventional proximity effect—are markedly suppressed[1]. On the one hand, the exchange field E_{ex} strongly limits the length $\xi_F = \sqrt{\hbar D/2E_{ex}}$ ($\xi_F = \hbar v_F/2E_{ex}$ for a ballistic system) over which the phase coherence of the electron/hole pair is maintained (Fig. 1b). In weak ferromagnets, ξ_F is only a few nanometres[16]. For the half-metallic F (H) $La_{0.7}Ca_{0.3}MnO_3$ (LCMO), $\xi_F < 1$ nm owing to the large $E_{ex} \sim 3$ eV (ref. 17). On the other hand, the Andreev-reflection probability is reduced owing to the spin-polarization of the conduction electrons in the F: in the extreme case of a H (100% spin-polarization), it is strictly forbidden owing to the zero density-of-states at the Fermi level within the minority-spin band, thereby hindering the penetration of superconducting correlations (Fig. 1c). However, if these could be sustained exclusively within the F majority-spin band, a long-range penetration comparable to ξ_N would be expected. Such equal-spin (triplet) correlations are foreseen in the presence of a so-called 'spin-active' S/F interface that induces spin-flip and spin-mixing processes[18,19]. From the microscopic point of view, an unconventional equal-spin Andreev-reflection process would be required for this type of triplet correlations to propagate into a H.

Our experimental approach to investigate these proximity effects consists of measuring the differential conductance of *c*-axis $Au/YBa_2Cu_3O_7/La_{0.7}Ca_{0.3}MnO_3$ (Au/YBCO/LCMO) and Au/YBCO/LCMO/YBCO micrometre-size junctions. The oxide heterostructures were grown by sputtering deposition and a series of lithography, etching, metal and isolator deposition steps were used to fabricate the vertical junctions sketched in Fig. 2 (see Supplementary Information for details on the sample preparation). Note that, contrary to the case of ramp-based junctions in which the *ab* plane of the cuprate is oblique to the S/F interface[20], in the present experiment the YBCO *ab* plane is parallel to it. We chose this geometry because it is exactly the one for which earlier experiments suggested long-range proximity effects across YBCO/LCMO interfaces[12,13]. Note also that, owing to the *ex situ* deposition of the top Au electrode, a relatively large Au/YBCO interface resistance is obtained that allows controlling—through the bias voltage V—the energy of the quasiparticles injected into the top YBCO (see Supplementary Section S3 for further details).

The low-temperature (3 K) conductance versus bias for a YBCO/LCMO/YBCO trilayer junction is shown in Fig. 2b (as we show later, a similar behaviour is also found for YBCO/LCMO bilayer junctions). The conductance is the numerical derivative of the measured $I(V)$ (inset). The background conductance shows

[1]Unité Mixte de Physique CNRS/Thales, 1 Avenue A. Fresnel, 91767 Palaiseau, France, [2]Université Paris Sud 11, 91405 Orsay, France, [3]GFMC, Dpto. Física Aplicada III, Universidad Complutense de Madrid, 28040 Madrid, Spain, [4]CEI Campus Moncloa, UCM-UPM, 28040 Madrid, Spain.
*e-mail: javier.villegas@thalesgroup.com.

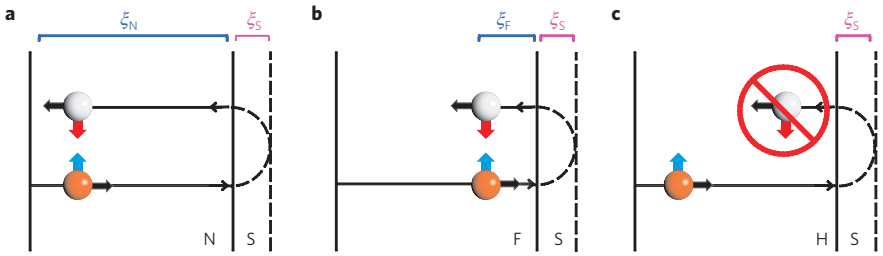

Figure 1 | Propagation of the superconducting correlations. a–c, Sketch of the propagation of the phase-correlated particles according to the conventional Andreev-reflection picture in which this is long-range in the case of a non-polarized N (**a**), short-range in the case of a F (**b**), forbidden in the case of a H (**c**). In the Andreev-reflection process the incoming electron penetrates the superconducting region as an electron-like quasiparticle within a distance ξ_S before being backscattered as a hole-like quasiparticle (with opposite spin) by the superconducting gap. This quasiparticle is subsequently transmitted back into the N or F as a hole. The distance over which phase coherence is maintained between the incident electron and the reflected hole is indicated as ξ_N in the N and ξ_F in the F.

a pronounced zero-bias peak, and rapidly decreases to become nearly flat as the bias is increased. Superposed to this background, a series of oscillations appears symmetrically for positive/negative bias, in a wide voltage range that largely exceeds the YBCO gap. The background conductance is similar to the one observed in junctions consisting of a single YBCO layer (see Supplementary Fig. S2 and related text), which evidences that it is essentially governed by the transport across the Au/YBCO interface. On the contrary, the conductance oscillations are specific to the presence of YBCO/LCMO interfaces. These resonances constitute the central finding of the present paper, and support the main conclusions. We argue below that they arise from electron and quasiparticle interference effects in the LCMO and YBCO layers.

We found that the conductance oscillations pattern is composed of two distinct sets of geometrical resonances, a long-period and a short-period one, which we respectively identified as Tomasch resonances[21,22] (TR) and McMillan–Rowell resonances[23,24] (MRR). Let us first describe these resonances in the general case of a N in contact with a S (Fig. 3a,b), the type of interface for which TR and MRR were early observed with conventional superconductors[21,23,24] and more recently with high-temperature d-wave ones[25–27]. The TR result from quasiparticle interferences in the S side of the interface. The interference (Fig. 3a) is between an incident electron-like quasiparticle (a 'mixture' of a hole and an electron in which the latter is predominant[15]) and its hole-like counterpart, which is Andreev-reflected back from the interface owing to the local perturbation of the energy gap[22]. The interference occurs for quasiparticle energies

$$V_n = \sqrt{\Delta^2 + (nh v_F^S / 2d_S)^2} \quad \text{with } n = 0, 1, 2, \ldots \qquad (1)$$

where Δ is the energy gap, v_F^S is the Fermi velocity in the S and d_S its thickness, and therefore shows in the conductance versus bias as a nearly periodic series of oscillations[22]. Conversely, the MRR arise as a consequence of resonances in the non-superconducting side of the interface. In this case (Fig. 3b), the incident electron is Andreev-reflected as a hole at the interface. However, unlike in the S (where the mixed character of quasiparticles allows for the interference between electron- and hole-like ones), in a non-superconducting material an electron and a hole cannot interfere[23]. Therefore, for the interference to occur in the N, the Andreev-reflected hole must subsequently travel a distance d_N to the opposite interface and, after being normal-reflected, propagate back to the S/N interface to undergo a second Andreev reflection. This returns the hole to its original electron state (Fig. 3b). Here it will interfere with the first incident electron, which gives rise to conductance oscillations with peaks at bias

$$V_m = V_0 + mh v_F^N / 4d_N \quad (\text{with } m = 0, 1, 2, \ldots) \qquad (2)$$

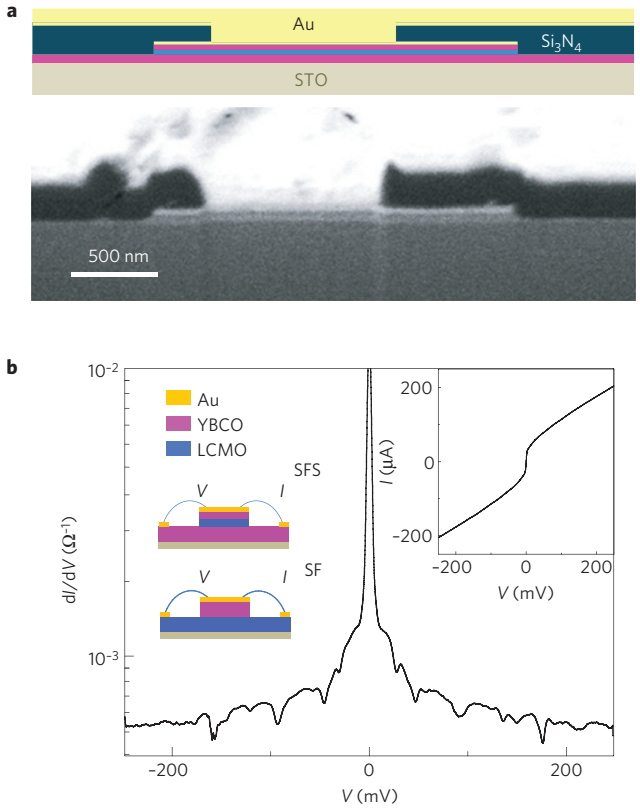

Figure 2 | Junction architecture and differential conductance. a, Scanning electron micrograph (bottom) of a SFS junction's cross-section made by focused ion-beam etching and its schematic representation (top). **b**, Differential conductance dI/dV as a function of the voltage V for the trilayer junction SFS2-J1 ($YBCO_{15\,nm}/LCMO_{12\,nm}/YBCO_{30\,nm}$) and sketch of the SFS and SF devices (left inset). Right inset: $I(V)$ characteristics from which the dI/dV has been obtained.

where v_F^N is the Fermi velocity in the N and d_N its thickness[23]. Note that the occurrence of MRR requires that the phase coherence induced by the energy gap between the incident electron and the Andreev-reflected hole is preserved while the latter travels back and forth a distance $2d_N$ (ref. 23). In other words, MRR imply that superconducting correlations survive in the N at least over that length scale. As a conclusion, the observation of MRR proves the occurrence of the superconducting proximity effect and can be used to measure its characteristic length scale.

We demonstrate in what follows the consistency of the analysis of the conductance oscillations observed in our samples—in which

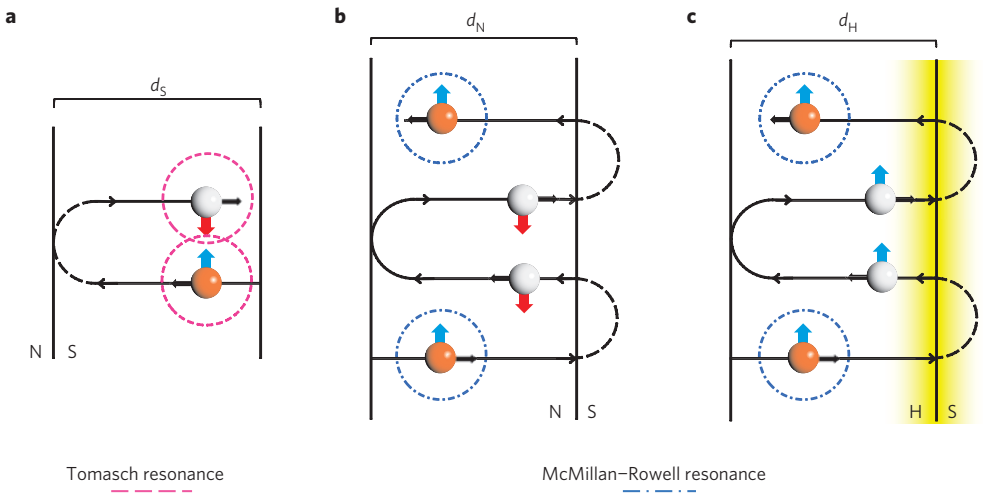

Figure 3 | Tomasch and McMillan–Rowell resonances. a–c, Schematic representation of the TR at a S/N interface (**a**), MRR at a S/N interface (**b**) and MRR at a S/H interface (**c**). The interfering particles are enclosed in the dashed and dot-dashed circles. Both TR and MRR require the Andreev reflection of the incident quasiparticle/electron, which at the S/H is possible only in the presence of a spin-active interface (shaded area in **c**) that flips the spin of the reflected particle. Note that in the superconducting side, an electron-like quasiparticle can interfere with its hole-like counterpart because each quasiparticle is a 'mixture' of both electron and hole states (one predominant over the other). Contrarily, in the non-superconducting side (N or H), particles have 'pure' electron (or hole) character, and can interfere only with particles of the same species.

a H instead of a N is in contact with the S—in terms of MRR and TR. For this, the conductance of YBCO/LCMO/YBCO and YBCO/LCMO junctions was compared, for several YBCO and LCMO thickness (the junctions parameters are listed in Table 1). Some examples of the experimental spectra are shown in Fig. 4a (black curves). Note that the background conductance has been numerically subtracted to emphasize the oscillation pattern. For each spectrum, the oscillation pattern results from the convolution of two series of oscillations: a long-period series (peaks marked with vertical lines) in which the oscillations have larger amplitude, and short-period series of smaller amplitude oscillations (see Supplementary Fig. S3). We found that the position of the conductance peaks in each of the two resonance sets respectively satisfies the TR and the MRR equations (1) and (2), if one assumes that TR occur in the top YBCO layer and MRR occur in the LCMO one. This assumption is justified because bilayer and trilayer junctions behave similarly, which implies that the bottom YBCO electrode does not play any role in the case of trilayer junctions. We obtained v_F^{YBCO} and v_F^{LCMO} from fits of the conductance peak positions V_n and V_m to equations (1) and (2)—Fig. 4b and c respectively—by using the YBCO and LCMO layers' thickness for d_{YBCO} and d_{LCMO}. Comparable values of v_F^{YBCO} and v_F^{LCMO} were consistently obtained for all of the different junctions (listed in Table 1). This is demonstrated in the insets of Fig. 4b,c, where the slope parameters obtained from the fits to the data sets in the main panels are shown as a function of $1/d_{YBCO}$ and $1/d_{LCMO}$, respectively. The linear relationships observed in the insets of Fig. 4b,c prove the consistency of the analysis, and further support the interpretation of the conductance oscillations in terms of MRR and TR. Notably, the average Fermi velocities $v_F^{LCMO} = (1.91 \pm 0.74)10^7\,cm\,s^{-1}$ and $v_F^{YBCO} = (4.44 \pm 0.26)10^7\,cm\,s^{-1}$ are within the range reported in the literature for LCMO (ref. 28) and for the different crystalline orientations of YBCO (refs 25,29). To illustrate how the convolution of the two sets of oscillations give rise to the experimental spectra, we simulated the conductance for different bilayer and trilayer junctions using a simple phenomenological model (see Supplementary Information for a description of the method). In essence, two analytic oscillating functions are summed whose periods are given by the values of v_F^{YBCO} and v_F^{LCMO} from the analysis above. The simulated curves, shown as magenta curves in Fig. 4a, closely reproduce the experimental ones.

Table 1 | Parameters of the measured junctions.

Parameter	Junction				
	SFS1-J1	SFS1-J2	SFS2-J1	SF-J1	SF-J2
T_c (K)	60	60	60	50	50
d_{YBCO} (nm)	15	15	15	30	30
$d_{bottom-YBCO}$ (nm)	30	30	30	-	-
d_{LCMO} (nm)	9	9	12	30	30
v_F^{YBCO} 10^7 (cm s^{-1})	4.35	4.7	4.25	4.38	4.55
v_F^{LCMO} 10^7 (cm s^{-1})	1.8	2	1.75	2.58	2.65
Δ (meV)	26	26	20	7.5	14
V_0 (meV)	9	14	8	9	11

T_c is the onset of the superconducting transition as measured from resistance versus T; d_{YBCO} and $d_{bottom-YBCO}$ are the thickness of the top and bottom YBCO layers, respectively; d_{LCMO} is the thickness of the LCMO. Parameters extracted from the analysis of the oscillations, as obtained from fits to equations (1) and (2): v_F^{YBCO} and v_F^{LCMO} are the Fermi velocities in the YBCO and LCMO, respectively; Δ is the YBCO energy gap; V_0 is the phase of the McMillan–Rowell oscillations.

We discuss in what follows the implications of observing MRR at the S/H interface, in which the role played by the spin of the interfering quasiparticles, electrons and holes is of capital importance and leads to the main conclusion of this paper. As explained above, in the conventional picture of the Andreev reflection, an incident electron becomes an electron-like quasiparticle as it penetrates the superconducting region and, within a distance ξ_S, is backscattered into an opposite-spin hole-like quasiparticle state by the energy gap. This quasiparticle is subsequently transmitted to the normal material as a hole. However, if one considers a H, the hole transmission is forbidden because its spin is opposite to the majority spin (that of the incident electron) and therefore it finds no available states (Fig. 1c). Consequently, MRR are not expected in a H in contact with a S. Their observation in the present experiments can be understood only if one considers that a spin-flip process operates at the interface that induces in the Andreev-reflected hole the same spin as the incident particle (that is, the majority spin). The resulting equal-spin Andreev reflection would make possible the MRR in the H (Fig. 3c). The required spin-flip process most likely originates

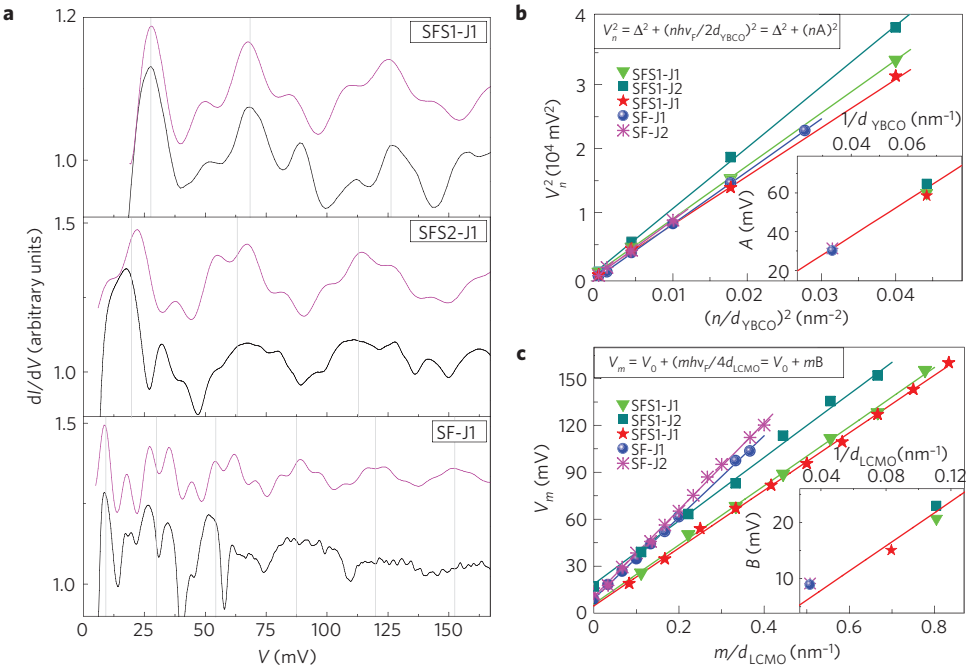

Figure 4 | Analysis of the conductance patterns. a, Conductance pattern dI/dV as a function of the voltage V after subtraction of the background (black curve) compared with the simulation (magenta curve) for (from top to bottom) SFS1-J1 trilayer junction ($YBCO_{15\,nm}/LCMO_{9\,nm}/YBCO_{30\,nm}$), SFS2-J1 trilayer junction ($YBCO_{15\,nm}/LCMO_{12\,nm}/YBCO_{30\,nm}$), SF-J1 bilayer junction ($YBCO_{30\,nm}/LCMO_{30\,nm}$). **b**, Position of the Tomasch maxima V_n^2 as a function of $(n/d_{YBCO})^2$, where n is the peak order and d_{YBCO} is the thickness of the top YBCO, for several junctions (see legend). The slope A^2 obtained from a linear fit to each data set allows us to calculate the Fermi velocity $v_F^{YBCO} = 2Ad_{YBCO}/h$, where h is the Planck constant. Inset: parameter A from the fits to the data sets in the main panel as a function of $1/d_{YBCO}$; the straight line is a linear fit from which we obtained the average v_F^{YBCO}. **c**, Position of the McMillan–Rowell maxima V_m as a function of m/d_{LCMO} where m is the peak order and d_{LCMO} the LCMO thickness. The slope B obtained from the linear fit to each data set in the main panel allows us to calculate the Fermi velocity $v_F^{LCMO} = 4Bd_{LCMO}/h$, where h is the Planck constant. Inset: slope B of the curves in the main panel as a function of $1/d_{LCMO}$; the straight line is a linear fit to the data from which we obtained the average v_F^{LCMO}.

at inhomogeneities of the magnetization[18,19], which are known to occur at interfaces involving cuprates and manganites[30]. In addition and importantly, the occurrence of MRR implies phase coherence between incident and reflected particles over a distance (at least) d_{LCMO}. In other words, the presence of MRR evidences the propagation of superconducting correlations into the LCMO at least over that distance. Given the values of d_{LCMO} up to 30 nm $\gg \xi_F$ (even if the ξ_F for weak ferromagnets was to be considered), those must necessarily be equal-spin triplet ones. Note that the last conclusion, which implies by itself the occurrence of equal-spin Andreev reflection, is irrespective of whether the LCMO polarization is strictly 100%.

Methods

The c-axis YBCO/LCMO heterostructures were grown on (001)-oriented $SrTiO_3$ single crystals in a high-O_2-pressure (3.4 mbar) d.c. sputtering system at 900 °C. These conditions yield a very slow (1 nm min^{-1}) and highly thermalized epitaxial growth. *In situ* annealing was done in 800 mbar O_2 pressure and 600 °C for 30 min. Further details on the growth and structural characterization of the YBCO/LCMO samples are given in the Supplementary Information. A top 50-nm-thick Au layer was d.c. sputtered *ex situ* after oxygen plasma preparation of the surface (10 W for 1 min). Vertical micrometre-size junctions of areas between 12 and 128 μm^2 were fabricated using standard photolithography techniques and ion etching. I(V) characteristics have been measured in a He-flow cryostat down to 1.8 K applying the voltage bias V (typically in the range ±200 mV) while measuring the current I.

Received 11 January 2012; accepted 16 April 2012; published online 13 May 2012

References

1. Buzdin, A. I. Proximity effects in superconductor-ferromagnet heterostructures. *Rev. Mod. Phys.* **77,** 935–976 (2005).
2. Keizer, R. S. *et al.* A spin triplet supercurrent through the half-metallic ferromagnet CrO_2. *Nature* **439,** 825–827 (2006).
3. Anwar, M. S., Czeschka, F., Hesselberth, M., Porcu, M. & Aarts, J. Long-range supercurrents through half-metallic ferromagnetic CrO_2. *Phys. Rev. B* **82,** 100501 (2010).
4. Khaire, T. S. *et al.* Observation of spin-triplet superconductivity in co-based Josephson junctions. *Phys. Rev. Lett.* **104,** 137002 (2010).
5. Robinson, J. W. A., Witt, J. D. S. & Blamire, M. G. Controlled injection of spin-triplet supercurrents into a strong ferromagnet. *Science* **329,** 59–61 (2010).
6. Sprungmann, D., Westerholt, K., Zabel, H., Weides, M. & Kohlstedt, H. Evidence for triplet superconductivity in Josephson junctions with barriers of the ferromagnetic Heusler alloy Cu_2MnAl. *Phys. Rev. B* **82,** 060505 (2010).
7. Senapati, K., Blamire, M. G. & Barber, Z. H. Spin-filter Josephson junctions. *Nature Mater.* **10,** 849–852 (2011).
8. Bergeret, F. S., Volkov, A. F. & Efetov, K. B. Odd triplet superconductivity and related phenomena in superconductor-ferromagnet structures. *Rev. Mod. Phys.* **77,** 1321–1373 (2005).
9. Eschrig, M. Spin-polarized supercurrents for spintronics. *Phys. Today* **64,** 43–49 (January 2011).
10. Dybko, K. *et al.* Possible spin-triplet superconducting phase in the $La_{0.7}Sr_{0.3}MnO_3/YBa_2Cu_3O_7/La_{0.7}Sr_{0.3}MnO_3$ trilayer. *Phys. Rev. B* **80,** 144504 (2009).
11. Fridman, I., Gunawan, L., Botton, G. A. & Wei, J. Y. T. Scanning tunneling spectroscopy study of c-axis proximity effect in epitaxial bilayer manganite/cuprate thin films. *Phys. Rev. B* **84,** 104522 (2011).
12. Kalcheim, Y., Kirzhner, T., Koren, G. & Millo, O. Long-range proximity effect in $La_{2/3}Ca_{1/3}MnO_3/(100)YBa_2Cu3O_{7-\delta}$ ferromagnet/superconductor bilayers: Evidence for induced triplet superconductivity in the ferromagnet. *Phys. Rev. B* **83,** 064510 (2011).
13. Sefrioui, Z. *et al.* Ferromagnetic/superconducting proximity effect in $La_{0.7}Ca_{0.3}MnO_3/YBa_2Cu_3O_{7-\delta}$ superlattices. *Phys. Rev. B* **67,** 214511 (2003).
14. Blonder, G. E., Tinkham, M. & Klapwijk, T. M. Transition from metallic to tunneling regime in superconducting microconstrictions: Excess current, charge imbalance, and supercurrent conversion. *Phys. Rev. B* **25,** 4515–4532 (1982).
15. Klapwijk, T. M. Proximity effect from an Andreev perspective. *J. Supercond. Novel Magn.* **17,** 593–611 (2004).
16. Cirillo, C. *et al.* Superconducting proximity effect and interface transparency in Nb/PdNi bilayers. *Phys. Rev. B* **72,** 144511 (2005).

17. Coey, J. M. D., Viret, M. & von Molnár, S. Mixed-valence manganites. *Adv. Phys.* **48,** 167–293 (1999).
18. Eschrig, M. & Löfwander, T. Triplet supercurrents in clean and disordered half-metallic ferromagnets. *Nature Phys.* **4,** 138–143 (2008).
19. Linder, J., Cuoco, M. & Sudbø, A. Spin-active interfaces and unconventional pairing in half-metal/superconductor junctions. *Phys. Rev. B* **81,** 174526 (2010).
20. Van Zalk, M., Brinkman, A., Aarts, J. & Hilgenkamp, H. Interface resistance of $YBa_2Cu_3O_{7-\delta}/La_{0.67}Sr_{0.33}MnO_3$ ramp-type contacts. *Phys. Rev. B* **82,** 134513 (2010).
21. Tomasch, W. J. Geometrical resonances and boundary effects in tunneling from superconducting. *Phys. Rev. Lett.* **16,** 16–19 (1966).
22. McMillan, W. L. & Anderson, P. W. Theory of geometrical resonances in the tunneling characteristics of thick films of superconductors. *Phys. Rev. Lett.* **16,** 85–87 (1966).
23. Rowell, J. M. & McMillan, W. L. Electron interference in a normal metal induced by superconducting contacts. *Phys. Rev. Lett.* **16,** 453–456 (1966).
24. Rowell, J. M. Tunneling observation of bound states in a normal metal-superconductor sandwich. *Phys. Rev. Lett.* **30,** 167–170 (1973).
25. Koren, G., Polturak, E. & Deutscher, G. Oxygen-controlled transition from tunnel-like to a weak-link behavior in $YBa_2Cu_3O_{7-d}/YBa_2CoCu_2O_y/YBa_2Cu_3O_{7-\delta}$ wedge-edge junctions. *Physica C* **259,** 379–384 (1996).
26. Nesher, O. & Koren, G. Observation of Tomasch oscillations and tunneling-like behavior in oxygen-deficient edge junctions. *App. Phys. Lett.* **74,** 3392–3394 (1999).
27. Nesher, O. & Koren, G. Measurements of Δ and v_F from Andreev reflections and McMillan-Rowell oscillations in edge junctions of $YBa_2Cu_3O_{6.6}/YBa_2Cu_{2.55}Fe_{0.45}O_y/YBa_2Cu_3O_{6.6}$. *Phys. Rev. B* **60,** 9287–9290 (1999).
28. Singh, D. J. & Pickett, W. Pseudogaps, Jahn-Teller distortions, and magnetic order in manganite perovskites. *Phys. Rev. B* **57,** 88–91 (1998).
29. Hass, N. *et al.* Sharp gap edge and determination of the Fermi velocity in $Y_1Ba_2Cu_3O_{7-\delta}$ by point contact spectroscopy. *J. Supercond.* **5,** 191–194 (1992).
30. Hoffmann, A. *et al.* Suppressed magnetization in $La_{0.7}Ca_{0.3}MnO_3/YBa_2Cu_3O_{7-\delta}$ superlattices. *Phys. Rev. B* **72,** 140407 (2005).

Acknowledgements

J.E.V. and C.V. wish to thank J. M. Rowell, A. Goldman and S. Maekawa for fruitful discussions. We thank C. Deranlot for Au deposition, D. Deneuve for technical support for the lithography process and C. Collet for focused ion beam and scanning electron micrographs. This work was supported by French ANR grant 'SUPERHYBRIDS-II' and RTRA grant 'Supraspin', European Community's FP7/2010 'Pixie', Spanish MICINN Grants MAT 2011 27470, CSD2009-00013 (IMAGINE) and CAM S2009-MAT 1756 (PHAMA).

Author contributions

J.E.V., J.S. and A.B. conceived the experiments. C.V. and J.T. grew the samples. C.V. performed the lithography processes. C.V., J.E.V. and Z.S. carried out transport experiments. C.V. analysed the data. C.V. and J.E.V. wrote the paper. All of the authors contributed to the discussion leading to the understanding of the data and contributed to the preparation of the manuscript.

Additional information

The authors declare no competing financial interests. Supplementary information accompanies this paper on www.nature.com/naturephysics. Reprints and permissions information is available online at www.nature.com/reprints. Correspondence and requests for materials should be addressed to J.E.V.